

Temporarily Coherent Scatterer Selection for Transport Infrastructure Monitoring with Sentinel-1 InSAR

Andreas PITER^{1,*}, Mahmud HAGSHENAS HAGHIGHI¹, and Mahdi MOTAGH^{1,2}

¹ *Institute of Photogrammetry and GeoInformation, Leibniz University Hannover, Germany*
(`{piter, mahmud}@ipi.uni-hannover.de`)

² *Helmholtz Centre Potsdam, GFZ German Research Centre for Geosciences, Germany* (`motagh@gfz-potsdam.de`)

* *corresponding author*

Abstract

Interferometric Synthetic Aperture Radar (InSAR) time series analysis enables cost-effective and long-term structural health monitoring of transport infrastructures. However, existing time series methods require the signal of a scatterer to remain coherent over the whole study period to estimate its displacement. With increasing operation time of Sentinel-1 less scatterers are continuously coherent, while the number of temporarily coherent scatterer (TCS) increases. Identifying the time interval TCS are valid at transport infrastructures is key for continuous monitoring. In this study we analyse state-of-the-art TCS detectors in the context of transport infrastructure monitoring and compare the approach for point-like scatterer (PS) pixels based on the amplitude time series with the approach for distributed scatterer (DS) pixels based on the structure of the coherence matrix. We provide a case study for an area west of Alicante, Spain, including demolished and re-constructed highway and bridge to evaluate the methods' performance on a Sentinel-1 stack covering the period from 2014 to 2024. Our results show that the change detected from the amplitude does not necessarily align with the coherent period of the infrastructure. The approach based on the coherence matrix outperforms the amplitude-based method, however at the cost of spatial resolution and computational time.

Keywords: InSAR, Temporarily Coherent Scatterer, Change detection, Transport infrastructure

Received: 9th December 2024. Revised: 24th February 2025. Accepted: 25th February 2025.

1 Introduction

Monitoring infrastructures is an important task in geodesy and can be achieved by wide-area measurements with mm to cm accuracy with spaceborne Interferometric Synthetic Aperture Radar (InSAR) (Crosetto et al., 2016). InSAR time series methods rely on scatterers which preserve coherent backscattering and allow the phase to be analysed. An ideal InSAR time series processing algorithm should be able to identify and discard non-coherent pixels to avoid errors. The selection of coherent pixels is a challenging task addressed by various approaches, e.g. based on amplitude statistics (Ferretti et al., 2001), spatial coherence (Berardino et al., 2002), assessment of phase noise (Hooper et al., 2007) or spatiotemporal scattering behaviour of neighbour-

ing pixels (Ferretti et al., 2011). The approaches commonly assume that the backscattering of a scatterer is coherent during the whole study period, i.e. in all acquired images. This has the advantage that all selected pixels can be unwrapped in the same manner during the InSAR time series analysis. Nevertheless, pixels which are incoherent in only a few acquisitions could also be identified which might introduce erroneous observations.

Existing pixel selection methods do not address this kind of scatterers that are not coherent during the study period, e.g. a bridge that is newly constructed. We call these pixels temporarily coherent scatterer (TCS). With increasing image stack size, e.g. meanwhile Sentinel-1 archives provide more than 10 years of data, the number of TCS increases and, in contrast, the number of scatterers

that maintain coherence throughout the entire period decreases due to changes in the scene. With traditional InSAR time series methods, newly constructed infrastructures necessitate InSAR processing of temporal subsets that align with the coherent time for each infrastructure or even a different temporal subset for each pixel.

To overcome this problem and to provide an InSAR time series framework for TCS, there have been developments particularly for urban infrastructures (Hu et al., 2019, 2021; Dörr et al., 2022). State-of-the-art TCS methods aim at identifying so called change points, i.e. a significant change in the signal time series due to a change in the scattering behaviour of the scatterer. Subsequently, the methods identify the coherent period of each TCS during InSAR time series analysis.

It is often assumed that a change of the surface within the resolution cell of the radar image leads to a change in the scattering mechanism, e.g. the construction or demolition of a building results in a significant increase or drop of the amplitude signal, respectively. In contrast to buildings, transport infrastructures such as highways exhibit low backscattering and existing TCS methods might not be applicable for this purpose. In this paper, we evaluate two state-of-the-art TCS methods for the specific application of transport infrastructure monitoring with Sentinel-1 InSAR namely those suggested by Hu et al. (2019) and by Monti-Guarnieri et al. (2018). Our contributions are: 1) Analysis of state-of-the-art TCS change detection methods for point-like scatterer (PS) and distributed scatterer (DS) pixels. 2) Performance assessment at a newly constructed highway and bridge. 3) Validation of the estimated change point with optical images and with InSAR displacement time series.

2 Change detection for TCS

Two state-of-the-art change detection methods to identify change points for TCS are discussed in this section. In Piter et al. (2024b), we showed that PS and DS are present on transport infrastructures. Here, we therefore apply a non-coherent change detector for PS pixels based on the amplitude time series (Hu et al., 2019) and a coherent change detector for DS pixels based on the coherence matrix (Monti-Guarnieri et al., 2018). Both methods require a stack of coregistered single-look complex (SLC) images.

Although multiple change points can be inferred by a recursive change detection (Hu et al., 2021; Manzoni et al., 2021), in this paper, we assume that there is only one change in the time series, because the recursive change point estimation might result in an over-segmentation of the time series which is not further discussed here. Finally, the coherent period of the signal can be inferred in the subsequent InSAR time series analysis.

The general workflow for change detection contains the following steps. The change of the scattering of a pixel can happen at any time during the study period. Hence, we define the set of change time candidates as all possibilities when a change could have occurred between two consecutive image acquisitions. We split the time series based on a change time candidate into two distinct subsets, and compute a test score from the time series of the subsets for each of the change detection methods. The test score represents the likelihood of a change at the current change time candidate. Finally, the time corresponding to the best test score - whether minimum or maximum, depending on the method - is selected as the change point for the pixel.

2.1 Changes in amplitude time series

The method proposed by Hu et al. (2019) assumes that a change in the scattering mechanism of a pixel results in a change in the amplitude signal, e.g. after a building is demolished the amplitude is significantly lower. Hence, this method identifies changes in the amplitude time series and classifies pixels that exhibit a change as TCS.

The method compares the distribution of two temporal subsets of the amplitude time series to test if they are significantly different. The amplitude of a PS pixel follows a Rice distribution, while incoherent pixels follow a Rayleigh distribution. Estimating the parameters of the Rice distribution for all possible combinations is time-consuming. Therefore, this method uses the Rayleigh distribution as its parameter is easy and fast to compute. The Rayleigh probability density function (PDF) of the amplitude A is given by

$$f(A | \sigma) = \frac{A}{\sigma^2} \exp\left(-\frac{A^2}{2\sigma^2}\right). \quad (1)$$

The scale parameter σ^2 is estimated from M independent samples of the amplitude time series

$$\hat{\sigma}^2 = \frac{1}{2M} \sum_{i=1}^M A_i^2. \quad (2)$$

A hypothesis test evaluates whether the two amplitude time series stem from the same Rayleigh distribution (null hypothesis H_0), which is the case if the scale parameter σ^2 is the same. Then, a potential change after acquisition n is validated through the test statistic F

$$F = \frac{\hat{\sigma}_1^2}{\hat{\sigma}_2^2} \underset{H_0}{\overset{H_1}{\gtrless}} F_{\alpha, 2n, 2(M-n)} \quad (3)$$

with the scale parameters $\hat{\sigma}_1^2$ and $\hat{\sigma}_2^2$ corresponding to the amplitude time series from acquisition 1 to n and $n+1$ to M , respectively. The test statistic follows the Fisher distribution with $2n$ and $2(M-n)$ degrees of freedom, and with significance level α .

2.2 Changes in coherence matrix structure

The method proposed by Monti-Guarnieri et al. (2018) models the structure of the coherence matrix of a DS pixel for the case of a change in the scattering mechanism. Originally, this method was developed for change detection in SAR images, e.g. for damage detection due to earthquakes. The concept is also applicable to InSAR time series analysis and we evaluate its applicability for transport infrastructure monitoring.

It is assumed that a DS pixel is surrounded by pixels with a similar scattering mechanism allowing for the estimation of the coherence matrix using the homogeneous neighbourhood. A scatterer which is coherent over the whole study period (e.g. covering five acquisitions) can be described by

$$\mathbf{C}_0 = \sigma^2 \begin{bmatrix} 1 & \gamma & \gamma & \gamma & \gamma \\ \gamma^* & 1 & \gamma & \gamma & \gamma \\ \gamma^* & \gamma^* & 1 & \gamma & \gamma \\ \gamma^* & \gamma^* & \gamma^* & 1 & \gamma \\ \gamma^* & \gamma^* & \gamma^* & \gamma^* & 1 \end{bmatrix} = \sigma^2 \mathbf{\Gamma}_0 \quad (4)$$

with the covariance matrix \mathbf{C}_0 , the coherence matrix $\mathbf{\Gamma}_0$, the coherence γ and its complex conjugate γ^* , and the variance σ^2 . A change in the scattering mechanism after acquisition n is assumed to result in two distinct coherent blocks which are not

correlated with each other

$$\mathbf{C}_n = \sigma^2 \begin{bmatrix} 1 & \gamma & \gamma & 0 & 0 \\ \gamma^* & 1 & \gamma & 0 & 0 \\ \gamma^* & \gamma^* & 1 & 0 & 0 \\ 0 & 0 & 0 & 1 & \gamma \\ 0 & 0 & 0 & \gamma^* & 1 \end{bmatrix} = \sigma^2 \mathbf{\Gamma}_n. \quad (5)$$

For simplicity, it is assumed that the variance σ^2 and the coherence γ are the same before and after the change. The likelihood $f(\mathbf{x} | \mathbf{C}_n)$ of a change after acquisition n is compared to the likelihood of no change $f(\mathbf{x} | \mathbf{C}_0)$ through the likelihood ratio test (LRT) in its logarithmic form

$$\log \frac{f(\mathbf{x} | \mathbf{C}_0)}{f(\mathbf{x} | \mathbf{C}_n)} = N_s \log \left(\frac{|\mathbf{\Gamma}_n|}{|\mathbf{\Gamma}_0|} \right) + N_s \text{Tr} \left((\mathbf{\Gamma}_0^{-1} - \mathbf{\Gamma}_n^{-1}) \hat{\mathbf{\Gamma}}_X \right) \quad (6)$$

with the vector of complex-valued observations \mathbf{x} , the modelled coherence matrices for change $\mathbf{\Gamma}_0$ and no-change $\mathbf{\Gamma}_n$, the coherence matrix $\hat{\mathbf{\Gamma}}_X$ estimated from the complex-valued vectors of N_s samples in the spatial neighbourhood of the scatterer, the matrix determinant $|\cdot|$, and the trace operator $\text{Tr}(\cdot)$. The LRT does not provide a PDF which could be used for statistical significance tests.

3 Experiments

Our study area is located west of Alicante in south-east Spain and features a highway and bridge that were newly constructed or reconstructed in recent years (cf. Fig. 1). The old highway and old bridge were demolished and reconstructed further south. The construction of the bridge took place between 2018 and 2021, and the highway was built between 2021 and 2023. The transport infrastructure in the study area is affected by different displacement signals at both, regional and local scale (Piter et al., 2024b).

We created a stack of 435 images from Sentinel-1 descending orbit track 8 showing the study area. The stack covers 10 years in the time span from 30-10-2014 to 09-07-2024. We chose a particularly low significance level of $\alpha = 0.0001$ for the F-test (cf. Eq. 3) on the amplitude time series to reduce the number of false-positive detections. We used the same coherence-level of $\gamma = 0.5$ as in Monti-Guarnieri et al. (2018) for the coherence matrix model (cf. Eq. 4 and 5) and estimated the coherence matrix from a 9×9 pixel neighbourhood.



Figure 1. Optical images covering the study area in southeast Spain (Plan Nacional de Ortofotografía Aérea (PNOA) from Instituto Geográfico Nacional, Spain: Images 2012 and 2021. ©Google, Airbus: 2023). The white lines in the map of 2012 indicate the location of the highway in 11/2024 (OpenStreetMap), i.e. the new highway is constructed south of the old one and the old bridge was replaced by a bigger one.

3.1 Results

3.1.1 Change index map

The method based on amplitude yields a heterogeneous change index map (cf. Fig. 2a). Correlations in the change index can be particularly found along the bridge and along certain sections of the highway. For 31 % of the pixels, no change point is detected due to insignificance of the F-test or missing data in the image. Those pixels are indicated as white in Fig. 2.

In contrast, the method based on the coherence matrix yields a more homogeneous change index map (cf. Fig. 2b) where neighbouring pixels have the same or similar change indices. We would expect similar change indices for pixels belonging to the same object. The transport infrastructure can be

clearly identified with a uniform change index along the whole highway and bridge. The change indices are in the range of 300 to 350 corresponding to 27-12-2020 to 10-11-2021, which is similar to the result from the amplitude-based method. However, the spatial window used for computing the coherence matrix results in high spatial correlation in the change indices due to spatial low-pass filtering effect. For 13 % of the pixels, no change index was estimated, either because of missing data in the original SLC or as the coherence matrix could not be estimated from its spatial neighbourhood in the boundaries of the image.

3.1.2 Test scores

We analysed the input data and the computed scores for the two change detection methods exemplarily for two pixels: one located at the bridge and the other one on the highway (cf. Fig. 5 for the location and the retrieved displacement time series of the two pixels). For the pixel on the highway (cf. Fig. 3), the change detection methods estimated different change points corresponding to 04-10-2020 (amplitude) and 24-08-2021 (coherence matrix). The amplitude time series after the change point has higher values than before the change point and the corresponding F-scores show one significant maximum. The LRT score of the change detection from the coherence matrix shows a clear minimum on 24-08-2021. The coherence matrix confirms the minimum by revealing a coherent block at the end of the time span while it is incoherent before the detected change point.

The pixel at the bridge (cf. Fig. 4) shows a diverse signal in both amplitude and coherence matrix compared to the pixel on the highway. The estimated change points are 07-04-2020 (amplitude) and 03-11-2020 (coherence matrix). Both amplitude and coherence matrix indicate three distinct temporal subsets exhibiting different amplitude signals and uncorrelated coherent blocks in the coherence matrix. The first covers the time span from 2015 to end of 2020. Subsequently, the second time span runs from the end of 2020 to the end of 2021, while the third covers the remainder of the study period. The first temporal subset is characterized by a high amplitude and a coherent block in the coherence matrix. The same applies to the last subset. In contrast, the second subset has lower amplitude and only two third of this time span is characterized by a coherent

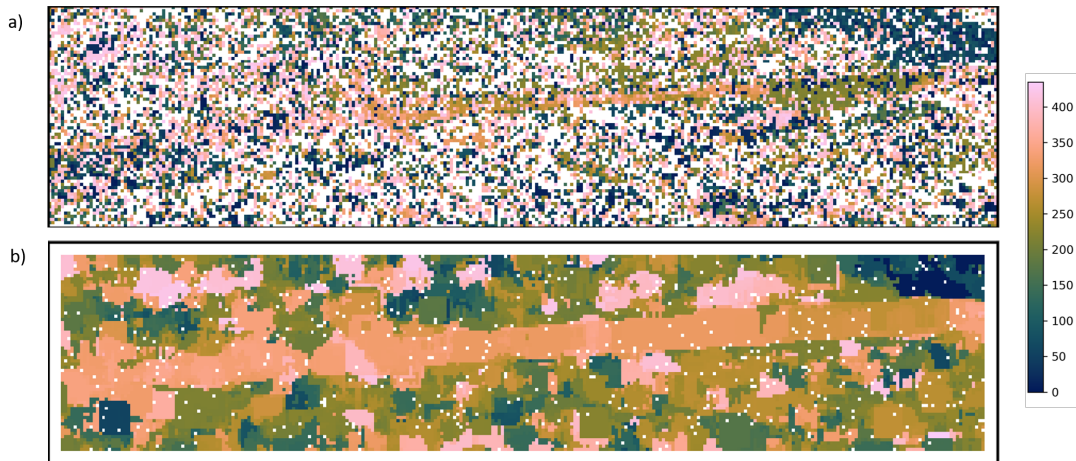


Figure 2. Change time index estimated from a) amplitude time series and b) coherence matrix. The coherence matrix could not be formed for pixels at the image borders, so these pixels are kept empty.

block in the coherence matrix. The change in amplitude is identified during the first time span at 07-04-2020 although a visual inspection does not suggest any distinct change. Beside the selected change point with an F-score of 2.37, there is a second significant local maximum with an F-score of 2.30 at 03-11-2020 which is the same change date as identified from the coherence matrix. This date coincides with the end of the first temporal subset. Comparing the change detection results with the optical images (cf. Fig. 1) reveals the existence of the old bridge during the first coherent period until mid of 2020, while the new bridge exists during the last coherent period starting in the end of 2021. The short period from 03-11-2020 to 25-06-2021 coincides with the construction time (cf. Fig. 1), which despite the construction activities preserves its coherence.

3.1.3 Displacement analysis

We estimate the displacement time series for two time spans: (a) the full study period from 30-10-2014 to 09-07-2024, and (b) the coherent time span from 13-07-2021 to 09-07-2024. We chose 13-07-2021 (acquisition index 330) as the start of the coherent time span based on two factors. First, the majority of the transport infrastructure in the study area shows a change point near this acquisition index. Second, the optical images confirm the change detection results and suggest that the construction work finished in between 2021 and 2023 for various segments of the transport infrastructure in the area. The displacement is retrieved with a single-reference interferogram network. Pixels that main-

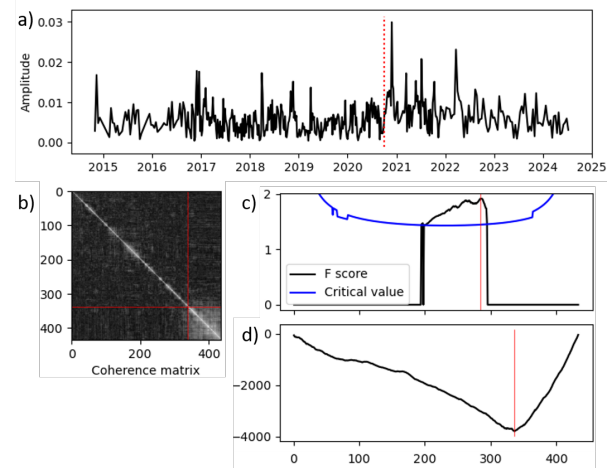


Figure 3. Example input data and scores for the pixel on the highway (white circle in Fig. 5b and the corresponding displacement time series in Fig. 5d). a) Amplitude time series. b) Coherence matrix (the coherence ranges from 0 (black) to 1 (white)). Scores computed from change detection methods for each potential change point index. c) F-scores estimated from amplitude time series. Non-significant F-scores have value zero. d) LRT scores estimated from coherence matrix. Red vertical lines in a) and c) indicate the change point from amplitude, while red lines in b) and d) show change point from coherence matrix.

tain coherence throughout the processing time span, which are considered useful targets for displacement analysis, are selected based on a temporal phase coherence (TPC) (Zhao and Mallorqui, 2019) threshold of 0.7. Consequently, their phases are

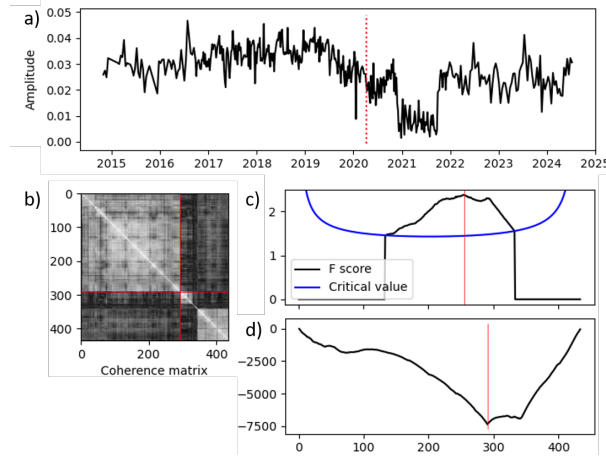


Figure 4. Example input data and scores for the pixel on the bridge (white circle in Fig. 5a and the corresponding displacement time series in Fig. 5c).

unwrapped in time and space (Piter et al., 2024b) with a one-step approach. The phase unwrapping max-flow (PUMA) method (Bioucas-Dias and Valadao, 2007; Boykov and Kolmogorov, 2004) is used for spatial phase unwrapping. The InSAR time series analysis is done using the open-source software SARvey (Piter et al., 2024a), the same processing parameters are chosen for both time spans.

The InSAR time series analysis for the full time span yields no coherent point on the highway in the displacement map (cf. Fig. 5a). In contrast, a few coherent points are identified on the northern part of the bridge. The scatterer on the bridge (circle in Fig. 5a) was considered in the InSAR time series analysis despite its three coherent periods (cf. Fig. 4). It shows the maximum displacement rate in the map with a LOS rate of -6 mm/year. The displacement time series (cf. Fig. 5c) has a negative slope for the time span from the end of 2016 until the end of 2020, but has a period of stability from 2022 to 2024. The jumps in the magnitude of half a wavelength of the microwave signal between the time series points suggest unwrapping errors which occur in the periods from 2014 to mid of 2015, and in the beginning of 2021. The period of 2021 to 2022 coincides with the construction time of the new bridge and the displacement time series of this period is characterized with a higher noise level. The displacement time series of this scatterer reflects the displacement from three different objects (old bridge, construction time and new bridge). This pixel highlights the necessity of considering the coherent period of TCS to avoid wrong interpretation

of the displacement results.

The displacement map derived for the coherent period (cf. Fig. 5b) shows a high density of coherent points along the highway and on the bridge. Parts of the highway show a spatially correlated LOS displacement with a rate of up to -19 mm/year. The scatterer with the maximum displacement rate within the study area is located at the highway and shows a linear pattern with cumulative displacement of -60 mm over three years (cf. Fig. 5d, circle in Fig. 5b).

3.2 Discussion

The change detection methods yield different results due to their different underlying assumptions. While both methods identified similar change times for pixels on the highway and at the bridge, the coherence matrix delivers a relatively uniform change time along the transport infrastructure, while the amplitude yields a more heterogeneous result. Considering that the construction work has spatial correlation, the results provided by the method based on the coherence matrix are more reasonable. Our results provide evidence that the amplitude method has limitations in identifying change points, as the change points are not correlated with construction time and location.

The validation with optical images suggests that the coherence matrix yields more precise change detection than the amplitude as the coherence is more sensitive to changes. Moreover, the coherence matrix already contains information on the coherent time span which is required for the InSAR time series analysis.

Despite these advantages, the method based on the coherence matrix comes with three drawbacks. First, the resulting change time map loses spatial details as the coherence matrix is estimated from a non-adaptive spatial window. As a result, a strong scatterer can dominate the change time index of other scatterers in its neighbourhood. Second, although the method was designed for DS pixels, it does not consider sources of decorrelation that influence the structure of the coherence matrix for a DS pixel. It works well for pixels with long-lasting high coherence, demonstrated as highly coherent blocks in the coherence matrix, which is rather found for PS pixels. Other literature, for example Costa et al. (2024), suggested non-parametric approaches to incorporate the decorrelation mechanism of DS pix-

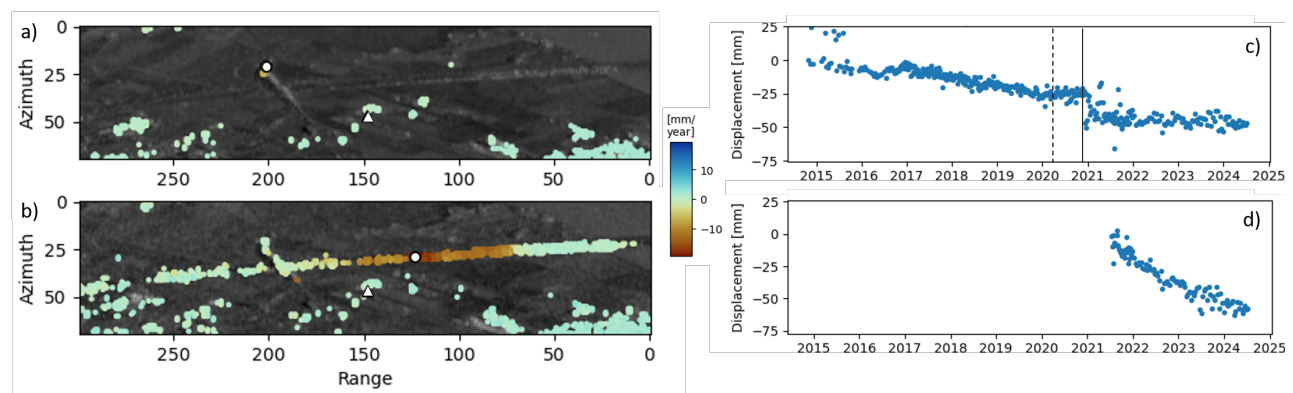


Figure 5. LOS displacement rate map estimated with SARvey (Piter et al., 2024a) for a) the full study period, and b) the coherent period. Positive values indicate displacement towards the sensor. The reference point is marked by the white triangle. The figures show the pixels in the SAR coordinate system, but flipped according to descending orbit. The background image is the amplitude signal averaged over the whole stack. Displacement time series for c) a pixel on the bridge (circle in a)), and d) a pixel on the highway (circle in b). The dashed line shows the change time from amplitude while the solid line depicts the change time from the coherence matrix.

els. However, such methods require a sequence of tests and heuristics to identify the change point. Nevertheless, the example of the pixel on the highway showed that the change detection is not sensitive to the model for the coherence matrix: The estimated change point coincides with the beginning of the coherent block although the coherence matrix does not fit to the underlying model for the change detection which assumes two coherent blocks with the same coherence level. Third, the coherence-based method is computationally intensive due to the inversion of large matrices, whose size depends on the number of images in the stack. The detection of change points based on the coherence matrix took approximately seven hours, compared to less than one minute for the amplitude-based change detection. Both methods were parallelized and processed on a computer with AMD EPYC 7601 32-Core CPU, 2.2 GHz and 256 GB RAM. Moreover, the determinant of the coherence matrix vanishes for a large matrix and the LRT becomes numerically instable.

The resulting change time maps show good agreement with the coherent time span inferred from high-resolution optical images. The displacement analysis also confirms the change detection results. While only 8 measurement points could be identified on the transport infrastructure for the whole study period, 609 points were detected after reprocessing according to the coherent time span.

The example scatterer on the bridge indicates prob-

lems in the change detection for scatterers with multiple change points and multiple coherent time spans.

4 Conclusion and outlook

In this paper, we presented the first analysis of temporarily coherent scatterer (TCS) for transport infrastructure monitoring with Sentinel-1. We evaluated two change detection methods based on the amplitude time series and on the structure of the coherence matrix. While the method based on the coherence matrix yields more precise change detection results and indicates the coherent time span, the amplitude time series can serve as a fast approximation for the change time. The results demonstrate the complexity of TCS in the context of transport infrastructures, mainly due to multiple coherent time spans that might occur for each pixel.

In future work, we will incorporate the identification of change point and estimation of the coherent period into a uniform workflow. Further, we will adapt the InSAR time series method to accommodate different coherent periods of individual TCS pixels.

Acknowledgements

The authors would like to thank Nils Dörr for the discussions on TCS. Results contain modified Copernicus data. Figures were created with QGIS,

Python, SARvey and the scientific colour maps (Cramer et al., 2020). A.P. received funding via the project SAR4Infra from the German Federal Ministry of Digital and Transport.

References

- Berardino, P., Fornaro, G., Lanari, R., and Sansosti, E. (2002). A new algorithm for surface deformation monitoring based on small baseline differential SAR interferograms. *IEEE Transactions on Geoscience and Remote Sensing*, 40(11):2375–2383.
- Bioucas-Dias, J. M. and Valadao, G. (2007). Phase Unwrapping via Graph Cuts. *IEEE Transactions on Image Processing*, 16(3):698–709.
- Boykov, Y. and Kolmogorov, V. (2004). An experimental comparison of min-cut/max-flow algorithms for energy minimization in vision. *IEEE Transactions on Pattern Analysis and Machine Intelligence*, 26(9):1124–1137.
- Costa, G., Monti-Guarnieri, A. V., Manzoni, M., and Rucci, A. (2024). A non-parametric estimator for Coherent Change Detection: the Permutational Change Detection. *IEEE Transactions on Geoscience and Remote Sensing*, pages 1–1.
- Cramer, F., Shephard, G. E., and Heron, P. J. (2020). The misuse of colour in science communication. *Nature Communications*, 11(1):5444.
- Crosetto, M., Monserrat, O., Cuevas-González, M., Devanthéry, N., and Crippa, B. (2016). Persistent scatterer interferometry: A review. *ISPRS Journal of Photogrammetry and Remote Sensing*, 115:78–89.
- Dörr, N., Schenk, A., and Hinz, S. (2022). Fully Integrated Temporary Persistent Scatterer Interferometry. *IEEE Transactions on Geoscience and Remote Sensing*, 60:1–15.
- Ferretti, A., Fumagalli, A., Novali, F., Prati, C., Rocca, F., and Rucci, A. (2011). A new algorithm for processing interferometric data-stacks: SqueeSAR. *IEEE Transactions on Geoscience and Remote Sensing*, 49(9):3460–3470.
- Ferretti, A., Prati, C., and Rocca, F. (2001). Permanent scatterers in SAR interferometry. *IEEE Transactions on Geoscience and Remote Sensing*, 39(1):8–20.
- Hooper, A., Segall, P., and Zebker, H. (2007). Persistent scatterer interferometric synthetic aperture radar for crustal deformation analysis, with application to Volcán Alcedo, Galápagos. *Journal of Geophysical Research: Solid Earth*, 112(B7).
- Hu, F., van Leijen, F. J., Chang, L., Wu, J., and Hanssen, R. F. (2021). Combined detection of surface changes and deformation anomalies using amplitude-augmented recursive InSAR time series. *IEEE Transactions on Geoscience and Remote Sensing*.
- Hu, F., Wu, J., Chang, L., and Hanssen, R. F. (2019). Incorporating Temporary Coherent Scatterers in Multi-Temporal InSAR Using Adaptive Temporal Subsets. *IEEE Transactions on Geoscience and Remote Sensing*, 57(10):7658–7670.
- Manzoni, M., Monti-Guarnieri, A., and Molinari, M. E. (2021). Joint exploitation of spaceborne SAR images and GIS techniques for urban coherent change detection. *Remote Sensing of Environment*, 253:112152.
- Monti-Guarnieri, A. V., Brovelli, M. A., Manzoni, M., Mariotti d’Alessandro, M., Molinari, M. E., and Oxoli, D. (2018). Coherent Change Detection for Multipass SAR. *IEEE Transactions on Geoscience and Remote Sensing*, 56(11):6811–6822.
- Piter, A., Haghshenas Haghighi, M., FERN.Lab, and Motagh, M. (2024a). SARvey - survey with SAR v1.1.0.
- Piter, A., Haghshenas Haghighi, M., and Motagh, M. (2024b). Challenges and Opportunities of Sentinel-1 InSAR for Transport Infrastructure Monitoring. *PFG – Journal of Photogrammetry, Remote Sensing and Geoinformation Science*, 92(5):609–627.
- Zhao, F. and Mallorqui, J. J. (2019). A Temporal Phase Coherence Estimation Algorithm and Its Application on DInSAR Pixel Selection. *IEEE Transactions on Geoscience and Remote Sensing*, 57(11):8350–8361.